Received: 29 September 2017 | Revised: 22 March 2018 | Accepted: 24 March 2018

DOI: 10.1002/eqe.3048

RESEARCH ARTICLE

WILEY

Dynamic behavior of a smart device on a surface subjected to earthquake motion

Yunsu Na[1] | Sherif El-Tawil[1] | Ahmed Ibrahim[2] | Ahmed Eltawil[2]

[1] University of Michigan, Ann Arbor, MI, USA

[2] University of California, Irvine, CA, USA

Correspondence
Sherif El-Tawil, University of Michigan, 2374 G.G. Brown, Ann Arbor, MI, USA.
Email: eltawil@umich.edu

Funding information
National Science Foundation, Grant/Award Numbers: 13624581362547, 1362458 and 1362547

Summary

This paper leverages concepts from an existing model to simulate the planar response of a smart device subjected to friction forces induced by an underlying moving plane. An interpolation technique is used to enhance detection of transition points (between sticking and sliding states), which must be accurately identified because of the frequency of their occurrence during seismic motion. The behavior of a smart device on an unconstrained table or desk, which is itself on a moving floor, is introduced and discussed. After validation of the results using experimental data, the revised model is used to study the sliding potential of smart devices on a surface during strong seismic events. Sliding spectra associated with selected ground motions are presented and extended to incorporate the effect of vertical accelerations with the purpose of assessing their influence. It is shown that vertical accelerations have a minimal effect on the sliding behavior of smart devices and that a "probability of exceeding the slip limit" curve can be developed to relate the probability of sticking to a demand parameter that represents the ground motion.

KEYWORDS

accelerometer, friction model, probability of exceeding the slip limit, sliding potential, smart device, stick-slip, transition point

1 | MOTIVATION AND INTRODUCTION

Dense networks of citizen-owned, internet-connected devices are now widespread in every major city in the world. Common examples of these devices are smart phones, tablets, laptops, and game consoles. Each of these devices is equipped with a motion sensor, or more specifically an accelerometer. These accelerometers generally are of reasonable quality and collect data continuously.[1]

The premise of this paper is that appropriately identified and processed acceleration data could be used to assess structural damage in the aftermath of an earthquake. In particular, the acceleration data can be integrated twice to yield floor displacements, which can be further processed to get interstory drift ratios along the building height (Li et al[2]). Comparing interstory drift ratio to well-known limits (eg, in FEMA 350 (2000)[3]) can provide insight into the damage that the building has experienced. Na et al[4] discussed the hurdles to achieving such a vision using commercially available smart devices. They noted that the errors in microelectromechanical system accelerometers, commonly used in smart devices, are too high and sampling rates low to permit accurate computation of displacements. However, a new generation of high-resolution, low-noise accelerometers, such as Nano-g[5] or nanoelectromechanical system (NEMS)[6] accelerometers, appears poised to enable smart devices to become accurate enough for use in earthquake damage assessment.

The first step in using smart devices as earthquake damage sensors is to develop an understanding of how they move during seismic shaking. The intent of this paper is to solve the governing equations of motion of a smart device sitting on a rigid flat base. For the sake of simplicity, a smart device is approximated as a rigid body (or block). The frictional response of an unconstrained block on a moving base can be divided into 2 main categories of behavior: sticking (presliding) and slipping (sliding).[7] The block transitions between sticking and slipping as the supporting base moves back and forth because of seismic excitation. At incipient sliding, in the so-called microslip zone, small relative motion occurs between the block and base.[8] The Stribeck (or velocity weakening) effect is characterized by a decrease in the friction force with increasing relative velocity, and frictional lag, where there is hysteresis in the friction versus velocity response. Once the applied inertial forces exceed the frictional resistance, the block moves beyond the microslip zone and starts sliding in earnest. Because of its importance to accurately compute the motion of the block, modeling "stick-slip" transition is a main concern in this work.

Numerous friction models are available in the literature, ranging from simple methods, which ignore key friction phenomena, to sophisticated ones that account for multiple considerations. The Coulomb law of dry friction is widely used in contact problems because of its simplicity. The Coulomb friction force, which acts opposite to the direction of motion of the body with respect to the moving base, is simply equal to the normal force between 2 bodies multiplied by the kinetic coefficient of friction.

To incorporate the Stribeck effect and the effect of presliding displacements, Canudas de Wit et al[9] proposed the LuGre model, which is an extension of the Dahl model.[10] This model is based on a bristle-like interpretation of the frictional interface. However, the LuGre model behaves like a linear spring/damper pair when it is linearized for small velocities, and as such, Parlitz et al[8] and Choi et al[11] criticized it as incapable of adequately considering presliding hysteresis. Lampaert et al[12] and Swevers et al[13] attempted to address this problem by incorporating a Maxwell slip model. However, the resulting models are complex and difficult to extend to 2 dimensions.

To simulate sticking and slipping behavior in contact problems with system damping and stiffness, Karnopp[14] developed a force-balance friction model for 1-dimensional motion. Beyond a predefined velocity window that signals when sliding is occurring, the friction force is described as a function of the sliding velocity. Tan and Rogers[15] extended Karnopp's 1-dimensional model to 2 dimensions. Their model exhibited "numerical chattering" in the velocity response when the tangential velocity was close to zero. To address this issue, Tariku and Rogers[16] introduced the concept of a microslip region, where the friction force acts opposite to the net external force, rather than the direction of the sliding velocity, which they argued is not reliable in this region. Based on this idea, they presented a new method to alleviate the chattering problem. In addition to a sticking spring, Tariku and Rogers[16] and Antunes et al[17] introduced a sticking damper when a sticking state is detected to eliminate the spurious local vibrations associated with the abrupt change in the friction force direction. However, the sticking damper properties, as well as the sticking spring properties, have no physical meaning.

Several categories of problems in earthquake engineering make use of friction models. Among the largest are base isolation systems and geotechnical engineering problems. Of particular interest to the ideas in this paper is the sliding behavior of monuments and blocks lying on the ground. For example, using Coulomb's law, Gazetas et al[18] introduced the idea of the "sliding potential" of a rigid block resting on horizontal or inclined planes subjected to horizontal and vertical motion. They used the sliding potential as a measure of the capacity of earthquakes to induce damage in sliding systems and introduced 1-dimensional sliding spectra of selected ground motion records. Other studies of sliding blocks can be found in Gazetas et al[19] and Westermo and Udwadia.[20] Most of the studies in this category of problems have focused on 1-dimensional problems and not 2, as done herein. Also, to the knowledge of the authors, this is the first study to focus on the behavior of smart devices.

In this paper, the Tariku and Rogers[16] model is modified and used to model the sticking and sliding behavior of smart devices on an underlying moving surface. The model is validated by comparing its behavior to experimentally measured data. After validation, the friction model is used to study the sliding potential of smart devices. Sliding spectra of selected records are provided for 2-dimensional motion and "probability of exceeding the slip limit" curves are subsequently derived, and their potential application discussed.

2 | FRICTION MODEL FOR AN UNCONSTRAINED SMART DEVICE

Figure 1A shows the system under consideration, where a block sits on a horizontal base. The base is subjected to some type of motion described by an acceleration time history, $\ddot{w}_x(t_n)$. The block on the base can undergo stick-slip motion

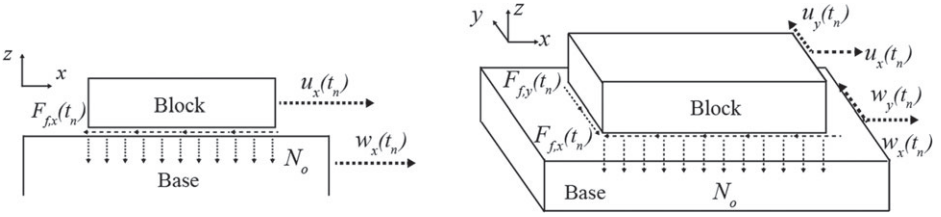

(A) One-dimensional motion **(B) Two-dimensional motion**

FIGURE 1 Problem setup: a block on a base

without restriction, ie, it is not constrained in any way. For simplicity, the normal load, N_o, is assumed a constant value, mg, where m is the mass of the block and g is the acceleration due to gravity. This assumption is relaxed later on in the paper, where variable vertical acceleration is taken into account. It is also assumed that the block and base are rigid and always in contact, ie, separation due to vertical acceleration does not occur. The equation of motion in the x direction is defined as:

$$m\ddot{u}_x(t_n) = F_{f,x}(t_n) \tag{1}$$

where $\ddot{u}_x(t_n)$ is the acceleration of the block in the x direction at time, t_n, and $F_{f,\,x}(t_n)$ is the friction force acting between the base and the block in the x direction. The solution of Equation (1) depends on the state of motion (sliding or sticking) and the friction model used. In 2 dimensions, the equation of motion is presented as follows:

$$\begin{aligned} m\ddot{u}_x(t_n) &= F_{fx}(t_n) \\ m\ddot{u}_y(t_n) &= F_{f,y}(t_n) \end{aligned} \tag{2}$$

where $\ddot{u}_y(t_n)$ is the acceleration of the block in the y direction at time, t_n, and $F_{f,\,y}(t_n)$ is the friction force acting between the base and the block in the y direction. For simplicity, the relative acceleration, velocity, and displacement between the base and the block in x and y directions at time (t_n) are defined as $\ddot{X}(t_n)$, $\ddot{Y}(t_n)$, $\dot{X}(t_n)$, $\dot{Y}(t_n)$, $X(t_n)$, and $Y(t_n)$, respectively.

2.1 | Modified sticking-spring-damper friction model

The friction model used in this paper is an extension of the model proposed by Tariku and Rogers[16] and Antunes et al.[17] Termed the sticking-spring-damper friction model (SSDFM), it is geared toward application to an unconstrained block (smart device) on a moving base subjected to seismic excitation. Two changes are made: (1) an interpolation technique is introduced to enhance detection of transition points, which occur frequently during seismic motion, and (2) the model is extended to handle vertical accelerations whereas the original model only considered constant vertical acceleration.

When sticking is detected, an imaginary tangential sticking spring with stiffness $K_{f,\,x}$ (in the x direction) and sticking damper with sticking damping coefficient $C_{f,\,x}$ (in the x direction) are inserted between the base and the bottom of the block. Combined, the sticking spring and damper force components represent the total friction force. The model detects sticking from sliding when 3 conditions are concurrently satisfied: (1) the relative velocity changes its sign, (2) the inertial force is less than the Coulomb static friction force, and (3) the sticking-spring-damper force is smaller than or equal to the Coulomb static friction force. When the sticking friction force is greater than the Coulomb static friction force, the sticking state is broken and sliding initiates and becomes governed by the kinetic friction force.

For 2-dimensional motion on a base, the sliding friction force in Equation (3) is divided into x and y components, parallel to those of the instantaneous sliding velocity unit vector, as follows:

$$\begin{bmatrix} F_{f,x}(t_n) \\ F_{f,y}(t_n) \end{bmatrix} = -\frac{\mu_k N_o}{\sqrt{\left(\dot{X}(t_n)\right)^2 + \left(\dot{Y}(t_n)\right)^2}} \begin{bmatrix} \dot{X}(t_n) \\ \dot{Y}(t_n) \end{bmatrix} \tag{3}$$

where μ_k is kinetic coefficient of friction and $F_{f,\,y}(t_n)$ is the friction force component in the y direction. This force distribution method is based upon the maximal dissipation rate principle[21] for isotropic situations.[22]

The transition from sticking to sliding commences when the magnitude of the external force (in this case inertial) is greater than the Coulomb static friction force. Following Tariku and Rogers,[16] it is assumed that the friction force acts opposite to the external force, rather than opposite to the direction of the sliding velocity in the microslip region, until the sliding velocity reaches 0.1 mm/second and has a consistent direction. The components of the friction force are calculated as a function of the acceleration vector as follows:

$$\begin{bmatrix} F_{f,x}(t_n) \\ F_{f,y}(t_n) \end{bmatrix} = \frac{\mu_k N_o}{\sqrt{\ddot{w}_x(t_n)^2 + \ddot{w}_y(t_n)^2}} \begin{bmatrix} \ddot{w}_x(t_n) \\ \ddot{w}_y(t_n) \end{bmatrix} \tag{4}$$

The set of equations is solved numerically using the Runge Kutta method.

Transition points are considered to occur when (1) sliding commences from sticking, (2) the sign of a component of the sliding direction reverses, and (3) sliding ends, leading to sticking. Using a constant time step for numerical simulations (as done in the traditional friction models) makes it difficult to find an accurate transition point. Instead of using the constant time step, an interpolation technique is applied to more accurately compute transition points and prevent overshooting. Therefore, at transition points, the time step is discretized into multiple substeps using a cubic spline. Experimentation with various numbers of steps showed that 20 substeps produce a reasonable answer as discussed later on in Section 3.

Figure 2 shows how the transition point is found. At transition, the velocities of the base and block are almost the same, and the block stops slipping or changes its slip direction depending on the friction forces at play. As shown in Figure 2, the larger time steps used during sliding (designated with stars [☆] in Figure 2) causes overshooting behavior. Once overshooting is detected (when the sign of relative velocity reverses), the solution process steps back to the last point before overshooting and restarts the computation with a smaller time step (1/20th of the original step) leading to more accurate detection of the transition point (designated first transition point in Figure 2). The smaller time steps are shown in Figure 2 as diamonds (◇). The larger time step is again reinstituted. As shown in Figure 2, the large time step again misses the transition point (second transition point in Figure 2). The interpolation process is repeated (shown by triangles [△] then circles (o) in Figure 2) to avoid excessive overshooting.

The SSDFM algorithm, which is based on Tariku and Rogers[16] and modified as outlined earlier, is applied at each time step t_n where n refers to the present time step and $n-1$ refers to the previous time as follows:

1 If the previous state at time t_{n-1} is sliding, then assess sticking by checking to see if the sign of the relative velocity changes. Compute β_x and β_y:

$$\begin{aligned} \beta_x &= \dot{X}(t_n)\cdot\dot{X}(t_{n-1}) \\ \beta_y &= \dot{Y}(t_n)\cdot\dot{Y}(t_{n-1}) \end{aligned} \tag{5}$$

1.1 If both β_x and β_y are positive, the system is still sliding. Compute friction forces from Equation (3).

1.2 If either one or both of β_x and β_y are zero or negative, compute the inertial force components, $F_{i,x}$ and $F_{i,y}$, acting on the block, and the Coulomb static friction force with static coefficient of friction, μ_s:

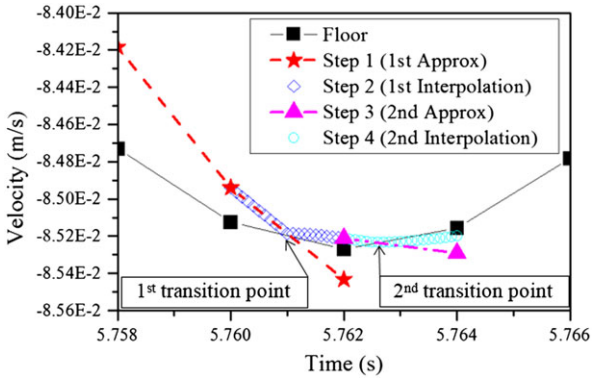

FIGURE 2 Detail of interpolation scheme to accurately identify transition points [Colour figure can be viewed at wileyonlinelibrary.com]

$$\begin{aligned} F_{i,x}(t_n) &= m\ddot{w}_x(t_n) \\ F_{i,y}(t_n) &= m\ddot{w}_y(t_n) \\ F_s &= N_o\mu_s \end{aligned} \tag{6}$$

1.2.1 If $\sqrt{(F_{i,x})^2 + (F_{i,y})^2} > F_s$, then the system is sliding. Compute the friction forces using Equation (3).

1.2.2 If $\sqrt{(F_{i,x})^2 + (F_{i,y})^2} \leq F_s$, then

1.2.2.1 Compute the transition points X_{st} and Y_{st} between $X(t_{n-1})$ and $X(t_n)$ and between $Y(t_{n-1})$ and $Y(t_n)$, respectively, by interpolation. Go back 1 step ($n = n - 1$) and restart the computation using Equation (3) with 1/20th of the original step until the transition points X_{st} and Y_{st} are reached, defined as the points where the sign of the relative velocity reverses.

1.2.2.2 Insert imaginary springs and dampers between the base and block in both x and y directions. Calculate sticking friction force components $F_{o,\,x}(t_n)$ and $F_{o,\,y}(t_n)$:

$$\begin{aligned} F_{o,x}(t_n) &= -K_{f,x}[X(t_n) - X_{st}] - C_{f,x}\dot{X}(t_n) \\ F_{o,y}(t_n) &= -K_{f,y}[Y(t_n) - Y_{st}] - C_{f,y}\dot{Y}(t_n) \end{aligned} \tag{7}$$

1.2.2.3 If $\sqrt{(F_{o,x}(t_n))^2 + (F_{o,y}(t_n))^2} > F_s$, the system is sliding. In this case, the friction forces are given by Equation (3).

1.2.2.4 If $\sqrt{(F_{o,x}(t_n))^2 + (F_{o,y}(t_n))^2} \leq F_s$, the system is sticking. Compute the sticking friction force by checking the conditions 1 step back:

1.2.2.4.1 If $\sqrt{(F_{o,x}(t_{n-1}))^2 + (F_{o,y}(t_{n-1}))^2} \geq \sqrt{(F_{f,x}(t_{n-1}))^2 + (F_{f,y}(t_{n-1}))^2}$, then the friction force becomes the sticking friction force $F_{f,\,x}(t_n) = F_{o,\,x}(t_n)$ and $F_{f,\,y}(t_n) = F_{o,\,y}(t_n)$.

1.2.2.4.2 If $\sqrt{(F_{o,x}(t_{n-1}))^2 + (F_{o,y}(t_{n-1}))^2} < \sqrt{(F_{f,x}(t_{n-1}))^2 + (F_{f,y}(t_{n-1}))^2}$, then go back 1 step ($n = n - 1$). Compute new $F_{o,\,x}(t_n)$ and $F_{o,\,y}(t_n)$ from Equation (7). Check for the sticking friction force as done in 1.2.2.4.1.

2. If the previous state at time t_{n-1} is sticking, then compare the sticking friction force computed from Equation (7) and the Coulomb static friction force F_s.

2.1 If $F_s \geq \sqrt{(F_{o,x}(t_n))^2 + (F_{o,y}(t_n))^2}$, the block continues to stick and the friction forces are computed from Equation (7).

2.2 If $F_s < \sqrt{(F_{o,x}(t_n))^2 + (F_{o,y}(t_n))^2}$, then sliding occurs.

2.2.1 If the relative velocities are greater than 0.1 mm/second, the friction force is given by Equation (3).

2.2.2 If the relative velocities are less than 0.1 mm/second, the friction force is given by Equation (4).

2.2 | Device on a table on a moving floor

The proposed friction model can be readily applied to the double stacked body problem as shown in Figure 3, where it is assumed that the smart device sits on a table or other piece of furniture, which in turn sits on a moving base. The table or furniture is assumed to be rigid body. The sliding criteria for double stacked bodies are presented as follows:

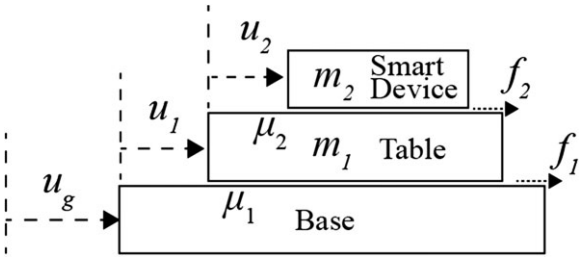

FIGURE 3 Schematic diagram of the double stacked bodies

$$|\ddot{u}_g| < \mu_1 g, |\ddot{u}_g + \ddot{u}_1| < \mu_2 g \tag{8}$$

where u_1 and u_2 are the relative displacements of the table with respect to the base and of the smart device with respect to the table, respectively, μ_1 and μ_2 are the coefficients of friction between the base and the table and between the table and smart device, respectively.

If the coefficient of friction between the table and block is higher than that between the base and the table ($\mu_2 > \mu_1$), the block does not slide with respect to the table. In other words, the table slides while the block sticks to it. The situation is more complex when $\mu_2 < \mu_1$. In this case, the table can slide with respect to the base and the block can also slide with respect to the table. Because the mass of the block is generally negligible with respect to that of the table, the problem can be uncoupled into 2 independent parts, where the motion of the table or block is computed as a function of the movement of the underlying surface. In either case, the motion can be computed using the algorithm in Section 2.1.

3 | PARAMETRIC STUDIES

Two key parameters, sticking spring stiffness and number of interpolation points, are studied to show how these parameters affect the simulation results. In the following, it is assumed that $m = 1$ kg, $\mu_s = 0.45$, $\mu_k = 0.4$, $N_o = 9.81$ N, and $C_{f,x} = 191$ N second/m. The time step of 0.1 millisecond is chosen to be less than 1 thousandth of the period of the highest frequency, among the natural, excited, and normal force frequencies as outlined in Tariku and Rogers.[16] The motion of the surface in the simulations is modeled using cosinusoidal functions with randomly generated amplitude and frequency. The amplitude range is 0.1 to 3 m/second, and the frequency range is 0.2π to 3π rad/second in the x and y directions, respectively. An error is defined as the deviation of the smallest computed sticking velocity of the block from the velocity of the base at the first transition from slipping to sticking. In the subsequent discussion, errors are normalized by dividing them by the maximum amplitude of the velocity record.

3.1 | Effect of the applied amplitude and sticking spring stiffness

Figure 4 shows the effects of the amplitude of the applied base velocity and the sticking spring stiffness of SSDFM on the normalized sticking velocity error. In Figure 4, the amplitude of the applied velocity ranges from 0.8 through 2.89 m/second, and the sticking spring stiffness ranges from 1000 to 80 000 N/m. Figure 4 shows that the sticking velocity errors of SSDFM decrease asymptotically as the sticking spring stiffness increases. It appears that increasing the sticking spring stiffness beyond 50 000 N/m does not result in significant reduction in the sticking velocity error. Also evident from Figure 4 is that selecting a larger amplitude for the cosinusoidal function results in a lower normalized sticking velocity error. In particular, the larger amplitude (2.89 m/second) function has a lower normalized sticking velocity than the smaller amplitude (1.30 and 0.80 m/second) functions.

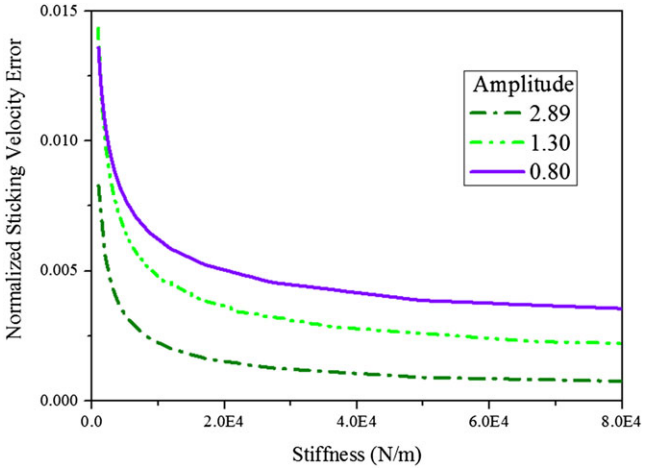

FIGURE 4 Effect of stiffness of spring and amplitude of applied velocity [Colour figure can be viewed at wileyonlinelibrary.com]

3.2 | Effect of the number of interpolation points

Figure 5 shows the effect of the number of interpolation points at the transition points on solution accuracy. It is clear that increasing the number of interpolation points results in a lower normalized sticking velocity error, but, of course, leads to longer computation time. Figure 5 shows that the rate of improvement in reducing the velocity error flattens out considerably at about 20 points, the number adopted in this work.

4 | COMPARISON TO EXPERIMENTAL RESULTS

Shake table experiments are conducted to show that the proposed model can reasonably represent the motion of an actual smart device on a seismically excited surface. The smart device selected is a Samsung Galaxy S7 (model SM-G930). The "Sensor kinetics pro" Android application by Innoventions, Inc., is used to record the phone's acceleration data. An infrared 3D motion capture system (Optotrak) is used to capture the true displacement of the smart device and shake table platen. The tracking system can monitor 3D positions of a set of markers with an accuracy of 0.1 mm and resolution of 0.01 mm at a distance of about 3 m. Two markers are placed on the platen, and another two are placed on the phone to measure the displacement time histories. Corresponding velocities and accelerations are obtained by differentiating the displacement data.

The shake table consists of a platen driven by a linear actuator and step motor. The latter is controlled by a step motor driver and the former an Arduino single-board microcontroller. LabView is used to feed signals to the shake table to simulate earthquake motion. The shake table can only represent 1-dimensional motion because of its configuration. Figure 6 shows the overall experimental setup with the smart phone, infrared sensors, shake table, platen, and Optotrak system.

Two sets of tests are conducted, one with the smart device encased in a polyurethane protective case and another without a case. The phone case type is selected because it has a high coefficient of friction with the platen to simulate sticking-dominant response. The bare phone has a much lower coefficient of friction with the platen, which results in sliding-dominant motion. Together, both sets of tests represent a wide range of possible situations. The measured static

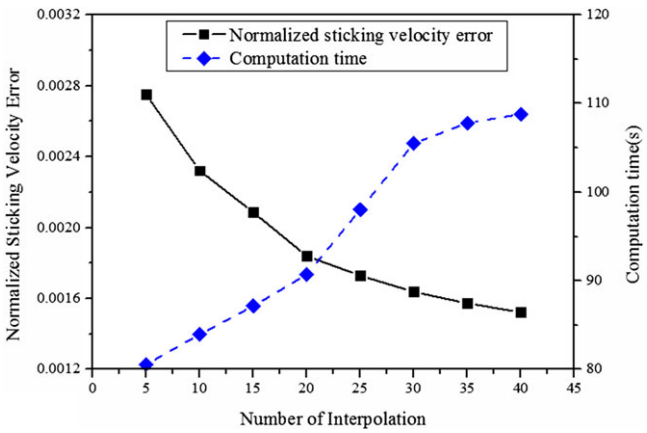

FIGURE 5 Effect of number of interpolation in the proposed model [Colour figure can be viewed at wileyonlinelibrary.com]

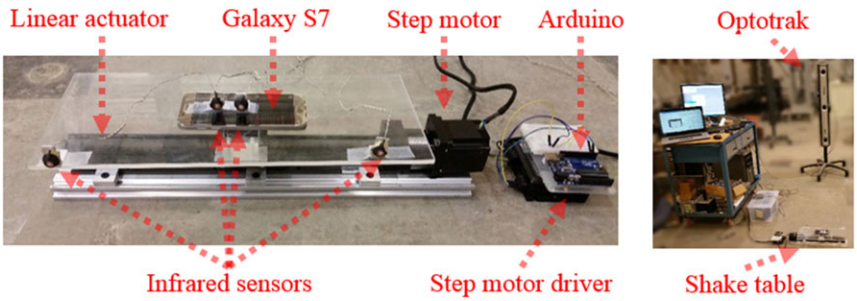

FIGURE 6 Experimental setup [Colour figure can be viewed at wileyonlinelibrary.com]

coefficient of friction between the shake table platen and polyurethane cover is 0.575, and the dynamic coefficient of friction is 0.384. The bare phone has a static coefficient of friction of 0.315 and a dynamic one of 0.210.

4.1 | Validation of proposed model

Simulation results from the proposed SSDFM are compared with the experimental results (from Optotrak and Galaxy S7) in Figure 7A, C. The input signals represent the strong motion portions of EQ2 and EQ3 in Table 1, accounting for 95% of the Arias Intensity. Because of minor surface imperfections in the platen, the measured acceleration during sliding motions is not a perfect plateau as computed in the numerical analysis as shown in Figure 7B, D. Nevertheless, the overall measured acceleration responses are quite close to the simulated acceleration responses.

The deviations between the measured acceleration from Optotrak and that from the smart device and between the measured acceleration from Optotrak and the simulated one from SSDFM are calculated by the root mean square error (RMSE) method. For both EQ2 and EQ3 motions, the smart device's measurements have more fluctuations during sliding motions compared to the SSDFM such that its RMSE is slightly higher than that for SSDFM. For EQ2 motion,

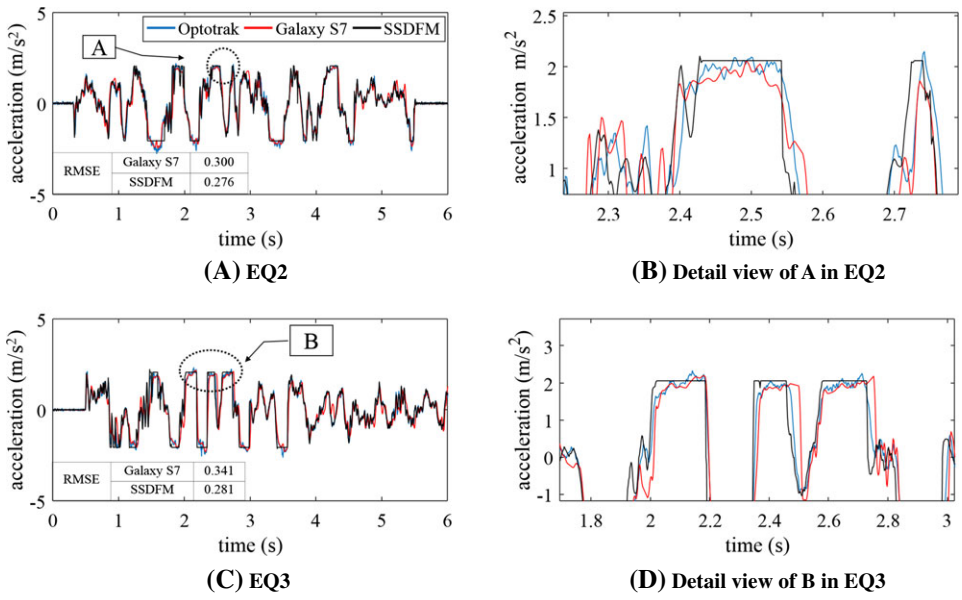

FIGURE 7 Comparison of RMSE of simulated and measured acceleration responses [Colour figure can be viewed at wileyonlinelibrary.com]

TABLE 1 Ground motion records used

	PEER-NGA Record Information		PGA (g)			Arias Intensity (I_A) (m/second)		
ID	Name	Record Seq. No.	*x* Direction	*y* Direction	*z* Direction	*x* Direction	*y* Direction	*z* Direction
EQ1	NORTHR/MUL	953	0.416	0.516	0.327	3.074	4.498	1.350
EQ2	NORTHR/LOS	960	0.410	0.482	0.318	1.913	1.976	0.532
EQ3	DUZCE/BOL	1602	0.728	0.822	0.203	3.724	2.431	0.485
EQ4	HECTOR/HEC	1787	0.266	0.337	0.150	0.831	1.866	0.353
EQ5	IMPVALL/H-DLT	169	0.238	0.351	0.145	2.398	3.290	0.538
EQ6	IMPVALL/H-E	174	0.364	0.380	0.140	3.918	3.227	0.511
EQ7	KOBE/NIS	1111	0.509	0.503	0.371	3.353	2.270	1.325
EQ8	KOBE/SHI	1116	0.243	0.212	0.059	0.827	0.639	0.059
EQ9	KOCAELI/DZC	1158	0.312	0.358	0.229	2.171	2.660	0.863
EQ10	KOCAELI/ARC	1148	0.219	0.150	0.086	0.578	0.434	0.223
EQ11	LANDERS/YER	900	0.245	0.152	0.136	0.231	0.169	0.113

the RMSE for the smart device is 0.300 compared to 0.276 for SSDFM. For EQ3 motion, the RMSE for the smart device is 0.341 versus 0.2810 for SSDFM.

Comparison between the location and number of sliding points as computed from SSDFM and measured in the experiments is another way to validate the model. The device without protective shell is used in the following discussion because it has a pronounced sliding response. Sliding motion is commonly assumed to occur when the relative velocity between the base and the device is greater than the Stribeck velocity v_s (0.001 m/second).[9] Based on the 0.002- second time step used in this study and given the displacement accuracy achievable by the Optotrak system, velocity can be measured to about 0.01 m/second.

Figure 8 illustrates the effect of the assumed v_s on the accuracy of state detection, ie, sliding versus sticking. The correct detection rate is the ratio of correctly matched states to the total number of states. The erroneous detection rate represents the remaining points. Figure 8 shows that the rate of increase in correct detections flattens out at around 0.012 m/second, which corresponds to the resolution of the test system. Hence, this number is adopted in this work to define the interface between sticking and sliding. Figure 9 plots sliding points for EQ2 and EQ3 as computed from

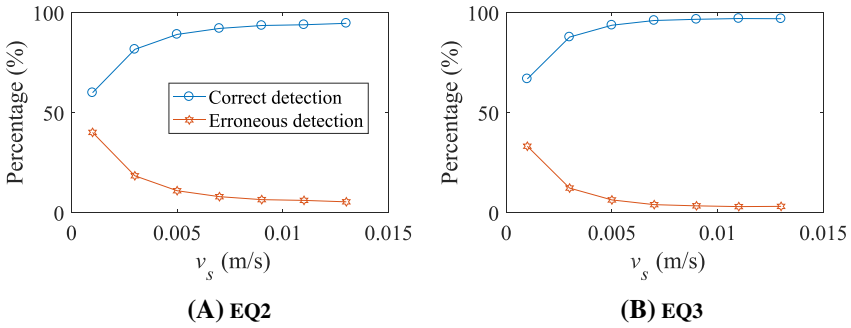

FIGURE 8 The effect of v_s on state detection [Colour figure can be viewed at wileyonlinelibrary.com]

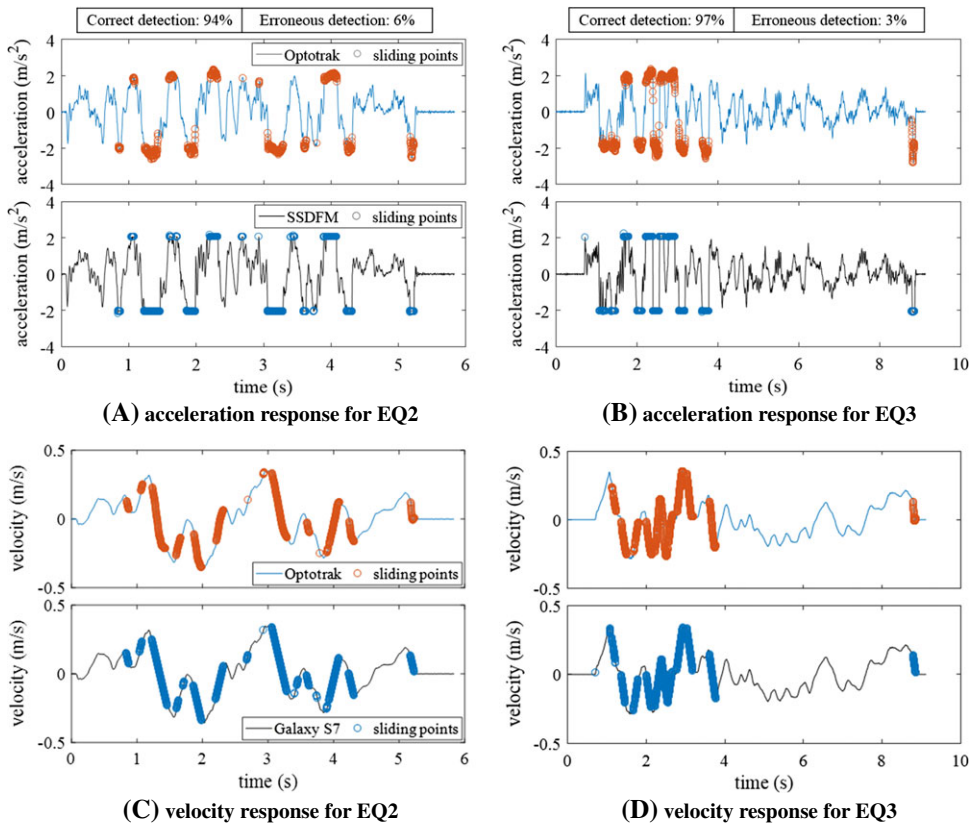

FIGURE 9 Comparison between measured and computed sliding points (v_s of 0.012 m/second) [Colour figure can be viewed at wileyonlinelibrary.com]

the Optotrak and SSDFM data. In Figure 9, sliding points are plotted as circles. It is clear that the measured data matches the computed data well. The high correct detection rate (94% for EQ2 and 97% for EQ3) signifies that the SSDFM is reasonably accurate and capable of modeling well the sticking and sliding regimes and the many transitions that occur between them.

5 | DYNAMIC RESPONSE OF SMART DEVICES UNDER EARTHQUAKE GROUND MOTION

Using the SSDFM developed earlier, the idea of sliding potential is used to assess the behavior of a rigid block on a horizontal base subjected to 2-dimensional motion and variable vertical acceleration. The intent is to identify under what conditions a smart device (block) will stick to the underlying surface under seismic action. The ground motions used in this study are from the far-field ground motion record sets in Federal Emergency Management Agency (FEMA).[23]

Table 1 lists their key characteristics, including peak ground acceleration (PGA) and the Arias Intensity (I_A) in 2 horizontal (x and y) and vertical (z) directions. The selected records are typically used by others for assessment of the probability of building collapse under the maximum considered earthquake as defined in ASCE/SEI 7-05.[24]

The critical acceleration is defined as the maximum acceleration the block can withstand without slipping. Based on this definition, the critical acceleration at which slip commences is:

$$A_c = |\mu_s g| \tag{9}$$

Whenever the magnitude of base acceleration,

$$\ddot{w} = \sqrt{\ddot{w}_x^2 + \ddot{w}_y^2} \tag{10}$$

exceeds A_c, sliding of the block initiates with respect to the base as mentioned in Equation (6).

5.1 | The effect of horizontal motion on the critical acceleration

Figure 10 shows the displacement response of the block in the horizontal plane when the underlying base is subjected to both components simultaneously of EQ1 and EQ2 and when $A_c = 0.1g$. It is clear from Figure 10B that the displacement response of the block subjected to the EQ2 ground motion has strong directivity in the x direction. Figure 11 shows the acceleration, velocity, and displacement responses in the x direction of EQ1 and EQ2 for $A_c = 0.1g$. The x component of EQ1 has a PGA of 0.416g, which is more than 4 times A_c, yet it produces a peak slip of only 0.060 m, which is less than half the peak displacement of the base (0.131 m). On the other hand, the x component of EQ2, which also has a PGA about 4 times A_c (PGA = 0.410g), has a peak sliding displacement of 0.226 m, which is about twice the peak displacement of the base (0.110 m). The main cause of this dichotomy is the relatively low-frequency content of EQ2 motion compared to EQ1, which allows the slipping action to build up for longer periods during EQ2.

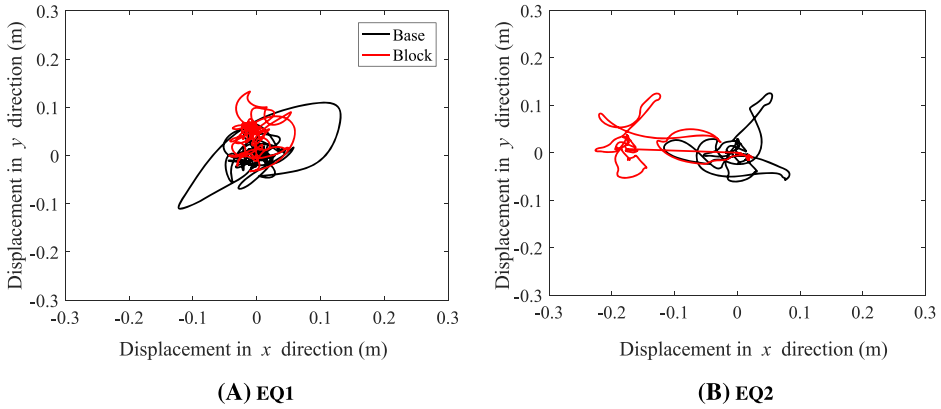

FIGURE 10 Sliding response induced by EQ1 and EQ2 when $A_c = 0.1g$ [Colour figure can be viewed at wileyonlinelibrary.com]

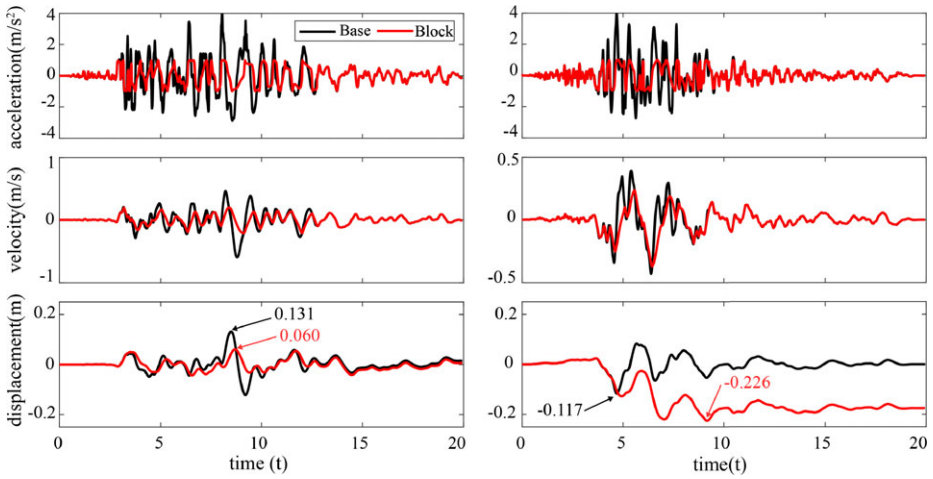

FIGURE 11 Sliding in the response induced by EQ1 and EQ2 when $A_c = 0.1g$ [Colour figure can be viewed at wileyonlinelibrary.com]

Table 2 shows a summary of the maximum drift ratios of the block and base for the 2 horizontal components of each record under horizontal motion. The maximum drift ratio is defined as the largest ratio of the peak displacement of the block to that of the base. Most of maximum drift ratios associated with horizontal motion only are close to unity with some exceptions, eg, EQ2 has a drift ratio of 1.933 in the x direction because of its high directivity in this particular direction.

5.2 | Effect of vertical motion

To account for the effect of vertical motion, which typically occurs during earthquakes, the assumption that the normal load is a constant value is relaxed. This is achieved by replacing Equations (3), (4), and (6) by the following 3 equations, respectively:

$$\begin{bmatrix} F_{f,x}(t_n) \\ F_{f,y}(t_n) \end{bmatrix} = -\frac{\mu_k m(g-\ddot{w}_z(t_n))}{\sqrt{\left(\dot{X}(t_n)\right)^2 + \left(\dot{Y}(t_n)\right)^2}} \begin{bmatrix} \dot{X}(t_n) \\ \dot{Y}(t_n) \end{bmatrix} \tag{11}$$

TABLE 2 Summary of maximum drift ratio for horizontal only and horizontal and vertical motions

Equation ID	Maximum Drift Ratio				Difference	
	Horizontal Ground Motion		Horizontal and Vertical Ground Motion			
	x Direction	*y* Direction	*x* Direction	*y* Direction	*x* Direction	*y* Direction
EQ1	0.456	1.197	0.45	1.308	1%	9%
EQ2	1.933	0.995	1.908	0.984	1%	1%
EQ3	0.934	1.383	0.937	1.392	0%	1%
EQ4	0.892	1.290	0.899	1.268	1%	2%
EQ5	1.014	1.014	1.010	0.995	0%	2%
EQ6	0.933	1.070	0.906	1.074	3%	0%
EQ7	0.993	0.912	0.905	0.941	9%	3%
EQ8	0.978	1.065	0.987	1.033	1%	3%
EQ9	0.875	0.988	0.878	0.957	0%	3%
EQ10	0.997	1.003	0.996	1.003	0%	0%
EQ11	1.139	1.015	1.139	1.011	0%	0%

$$\begin{bmatrix} F_{f,x}(t_n) \\ F_{f,y}(t_n) \end{bmatrix} = \frac{\mu_k m(g - \ddot{w}_z(t_n))}{\sqrt{\ddot{w}_x(t_n)^2 + \ddot{w}_y(t_n)^2}} \begin{bmatrix} \ddot{w}_x(t_n) \\ \ddot{w}_y(t_n) \end{bmatrix} \tag{12}$$

$$F_s = m(g - \ddot{w}_z(t_n))\mu_s \tag{13}$$

where $\ddot{w}_z(t_n)$ is the vertical acceleration time history. For the sake of simplicity, it is still assumed that the block remains in contact with the base, ie, no separation occurs, which is essentially true for all the ground motions consider herein because none of them had a vertical acceleration greater than the gravity acceleration.

The effect of vertical motion on the maximum drift ratio is summarized in Table 2. Figure 12 shows the displacement record of the 2 records with largest vertical peak accelerations: EQ1 and EQ7. It is clear from the Figure 12 that the effect of vertical motion is small. Figure 12 shows the same general trend. This can be seen by comparing the maximum drift ratios computed with and without vertical motion, where the maximum difference is generally within 2%, with the exception of a few cases, eg, the y component of EQ1 and the x component of EQ7. Others have also observed this effect in sliding systems, eg, in Gazetas et al and Sarma and Scorer.[19,25]

5.3 | Effect of critical acceleration

The effect of the critical acceleration is studied by varying A_c from 0.05g to 0.50g with increments of 0.025. The spectra of the maximum relative velocity between the base and the block of all the horizontal ground motions are plotted in Figure 13. It is can be seen from Figure 13 that the general trend is less slip with increasing A_c, becoming asymptotic with zero especially beyond $A_c = 0.3g$, ie, the block sticks to the base beyond this point. However, a number of obvious exceptions seem to occur, where the maximum relative velocity actually increases as A_c increases before eventually proceeding in the expected direction. This observation is known as the "Safe Gulf Paradox."[18]

The sticking critical acceleration is defined as the critical point where the maximum relative velocity is less than 0.001 m/second (the aforementioned Stribeck velocity). The intent of defining the sticking critical acceleration is to define the conditions under which the block sticks, from a practical perspective, to the base for a given earthquake intensity. These sticking A_c values are marked with a circle in Figure 13.

6 | PROBABILITY OF EXCEEDING THE SLIP LIMIT

If a sturdy (rigid) desk in a building has a high coefficient of friction and sticks to the floor, eg, it sits on a carpet that is firmly attached to the floor, its movements during an earthquake are representative of the motion of the underlying floor. The same idea can be extended to a smart device. If the device is in a protective shell made of a rubber-like polyurethane and there is a sufficiently high coefficient of friction between the shell and table to make it stick to the table during motion of the table, then the device's movements are represented of the table's movements, and therefore the underlying floor's movements. If, on the other hand, the coefficient of friction is not high enough or if the demand is too high, slip will likely occur and it becomes more challenging to assess the motion of the underlying floor from the device's readings. It is helpful to know the chance of this occurring.

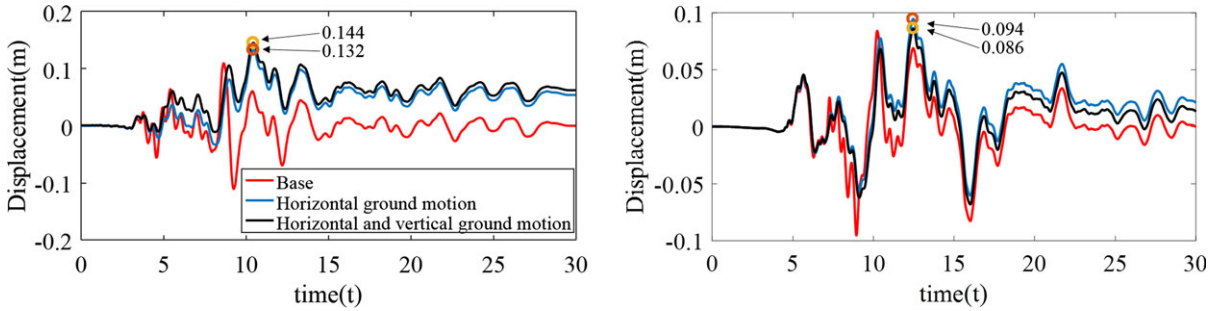

(A) EQ1 in *y* direction **(B) EQ7 in *x* direction**

FIGURE 12 Displacement response of a block subjected to the 2 records with the highest peak vertical acceleration [Colour figure can be viewed at wileyonlinelibrary.com]

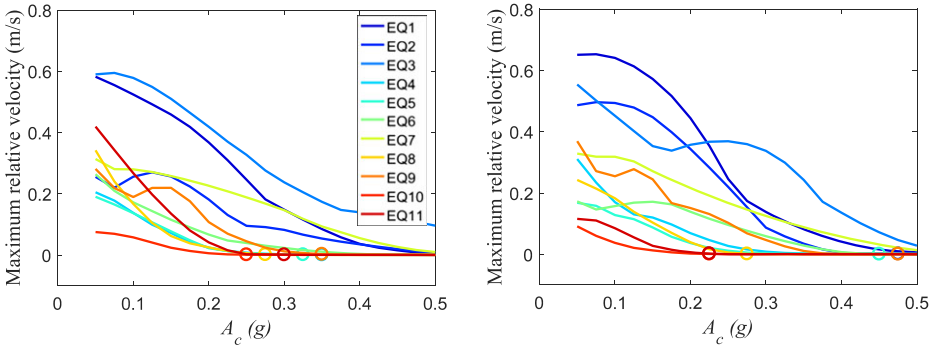

(A) In x direction (B) In y direction

FIGURE 13 Sliding spectra of the block in maximum relative velocity for all the horizontal ground motions with varying A_c [Colour figure can be viewed at wileyonlinelibrary.com]

Consider a 4-story steel frame building[26] with a first mode period of 1.67 seconds with 2.5% damping located in Seattle with latitude (34.049) and longitude (−118.252). Using hazard curves from the US Geological Survey (USGS), scale factors are computed by following the scaling method in Federal Emergency Management Agency (FEMA)[23] to generate new records that correspond to 3 hazard levels: 2% in 50 years, 10% in 50 years, and 50% in 50 years. The first period spectral accelerations corresponding to the 3 hazard levels are 0.55g, 0.26g, and 0.07g, respectively. To enrich the computational space, 4 additional spectral accelerations, 0.04g, 0.12g, 0.35g, and 0.45g (not tied to any specific hazard level), are used in the scaling scheme for a total of 7 scaled records for each earthquake. The scaled records are used to compute 4 maximum slip curves that correspond to critical acceleration values of A_c = 0.2g, 0.3g, 0.4g, and 0.5g. The sliding spectra of the block in maximum slip displacement between the base and the block for x and y components of all the horizontal ground motions are plotted in Figure 14. It is can be seen from Figure 14 that the general trend is that, aside from cases that follow the Safe Gulf Paradox,[18] the maximum slip decreases with increasing A_c.

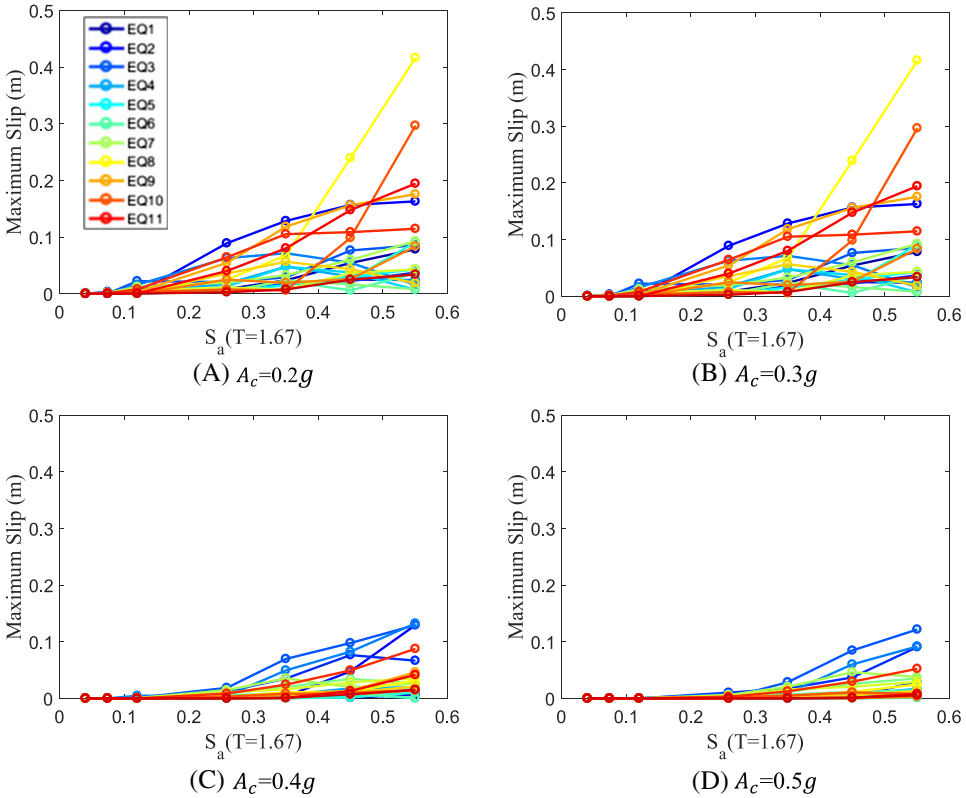

(A) A_c=0.2g (B) A_c=0.3g

(C) A_c=0.4g (D) A_c=0.5g

FIGURE 14 Sliding spectra of the block in maximum slip for all the horizontal ground motions with varying A_c [Colour figure can be viewed at wileyonlinelibrary.com]

TABLE 3 Probability of exceeding the slip limit for selected spectral accelerations and critical accelerations

Sa (T = 1.67 second)	A_c = 0.2g	A_c = 0.3g	A_c = 0.4g	A_c = 0.5g	Hazard Level
0.04 g	0%	0%	0%	0%	
0.07 g	0%	0%	0%	0%	50% in 50 years
0.12 g	9%	0%	0%	0%	
0.26 g	45%	18%	0%	0%	10% in 50 years
0.35 g	82%	36%	18%	18%	
0.45 g	91%	55%	18%	18%	
0.55 g	100%	64%	55%	36%	2% in 50 years

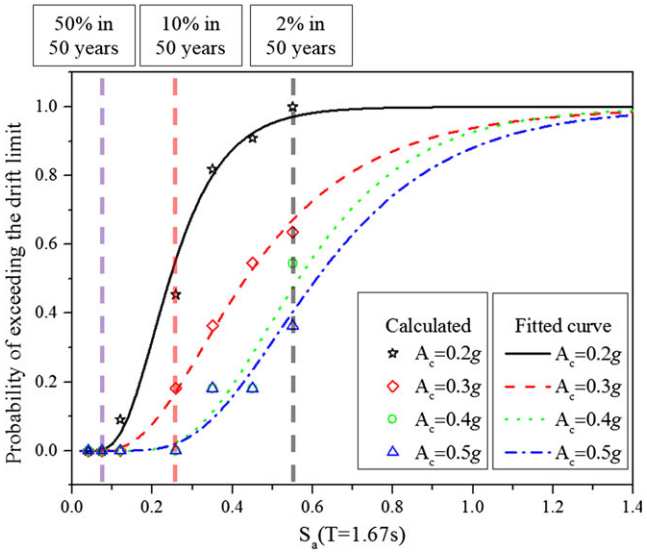

FIGURE 15 Probability of exceeding the slip limit as a function of the acceleration response spectrum for various critical accelerations [Colour figure can be viewed at wileyonlinelibrary.com]

Based on the information in Figure 14, the idea of a probability of exceeding the slip limit (PESL) curve is introduced. The PESL curve is analogous to a fragility function. The slip limit, which is the difference between the absolute values of the peak displacements achieved by the block and underlying base, is selected to be 0.02 m. This value corresponds to 10% of the interstory drift associated with the collapse prevention limit state. The selection of 0.02 m is essentially arbitrary and can be tightened or relaxed depending on the accuracy sought. The PESL curve is obtained by using the FEMA P-58 Conditional Probability of Collapse Curve Fit Tool[27] and relates the probability of slip of an unconstrained block to the first period spectral acceleration. Table 3 summarizes the calculated probability of exceeding the slip limit for selected 7 spectral accelerations with various critical accelerations. Figure 15 shows the fitted curve of probabilities for acceleration response spectrum with various value levels of A_c by using the curve fit tool. For example, for a 50% in 50-year event, there is no chance of exceeding the slip limit for all values of A_c. That grows to 36% for a 2% in 50-year event when $A_c = 0.5g$. The data in Table 3 and Figure 15 suggests that a device with a coefficient of friction of 0.4 will be capable of reading the movement of the underlying surfaces with a maximum slip of less than 0.02 m for events with 10% and 50% chances of occurrence in 50 years. This information (and the PESL curve, in general) can be useful for crowdsourcing damage assessment through smart devices after seismic events.

7 | CONCLUSION

The behavior of a smart device on an underlying surface subjected to seismic motion was investigated. The smart device was modeled as a rigid block, and its frictional interactions with the underlying base was represented using an existing

model that was modified for the purposes of this research. The revised model used an interpolation technique to enhance detection of transition points, which must be accurately detected because of the frequency of their occurrence during seismic motion. The second modification entailed extending the model to handle vertical accelerations. The behavior of a device on (rigid) furniture, which itself is placed on a floor subjected to seismic motion (double stacked problem), was also discussed.

After validation of the model by comparing its behavior to experiments, the sliding/sticking behavior of a smart device on a base subjected to seismic motion was investigated. In particular, the sliding spectra associated with selected ground motions were presented. It was shown that vertical accelerations have a small effect on the sliding behavior of smart devices. The concept of a probability of exceeding the slip limit curve was introduced and used to relate the probability of exceeding a given slip limit versus first period spectral acceleration for a given structure and location. Once generalized by taking into account other structures and locations, this information can be of value in future crowd-sourced, postdisaster reconnaissance efforts.

ACKNOWLEDGEMENTS

The authors acknowledge the financial support of the National Science Foundation under award numbers 1362547 and 1362458. Any opinions, findings, conclusions, and recommendations expressed in this paper are those of the authors and do not necessarily reflect the views of the sponsor. The authors are grateful to Tung-Yu Wu of the Civil and Environmental Engineering at University of Michigan for his academic discussions and extensive help.

ORCID

Yunsu Na http://orcid.org/0000-0003-3297-4822
Sherif El-Tawil http://orcid.org/0000-0001-6437-5176
Ahmed Ibrahim http://orcid.org/0000-0003-4002-4173
Ahmed Eltawil http://orcid.org/0000-0003-1849-083X

REFERENCES

1. Dashti S, Bray JD, Reilly J, Glaser S, Bayen A, Mari E. Evaluating the reliability of phones as seismic monitoring instruments. *Earthq Spectra*. 2014;30(2):721-742. https://doi.org/10.1193/091711EQS229M
2. Li H, Dong S, El-Tawil S, Kamat V. Relative displacement sensing techniques for postevent structural damage assessment: Review. *J Struct Eng*. 2012;356(September):1421-1434.
3. Federal Emergency Management Agency (FEMA). *Recommended seismic design criteria for new steel moment-frame buildings. FEMA-350*. Washington, D.C: Prepared by the SAC Joint Venture for FEMA; 2000.
4. Na Y, El-Tawil S, Ibrahim A, Eltawil A. The feasibility of using smart devices for quantifying seismic damage to buildings. Structures Congress 2017, 2017. https://doi.org/10.1061/9780784480427.
5. Khoshnoud F, De Silva CW. Recent advances in MEMS sensor technology-mechanical applications. *IEEE Inst Meas Mag*. 2012;15(2):14-24. https://doi.org/10.1109/MIM.2012.6174574
6. Barbour N, Schmidt G. Inertial sensor technology trends. *IEEE Sens. J*. 2001;1(4):332-339. https://doi.org/10.1109/7361.983473
7. Hsieh C, Pan YC. Dynamic behavior and modelling of the pre-sliding static friction. *Wear*. 2000;242(1-2):1-17. https://doi.org/10.1016/S0043-1648(00)00399-9
8. Parlitz U, Hornstein A, Engster D, et al. Identification of pre-sliding friction dynamics. *Chaos: Interdiscipl J Nonlinear Sci*. 2004;14(2):420-430. https://doi.org/10.1063/1.1737818
9. Canudas De Wit C, Aström KJ, Lischinsky P. A new model for control of systems with friction. *IEEE Transact Automat Contr*. 1995;40(3):419-425. https://doi.org/10.1109/9.376053
10. Dahl P. Solid friction damping of spacecraft oscillations. Proc of AIAA Guidance and Control Conference, 1975. https://doi.org/10.2514/6.1975-1104.
11. Choi JJ, Han SI, Kim JS. Development of a novel dynamic friction model and precise tracking control using adaptive back-stepping sliding mode controller. *Mechatronics*. 2006;16(2):97-104. https://doi.org/10.1016/j.mechatronics.2005.10.004
12. Lampaert V, Swevers J, Al-Bender F. Modification of the Leuven integrated friction model structure. *IEEE Transact Automat Contr*. 2002;47(4):683-687. https://doi.org/10.1109/9.995050

13. Swevers J, Al-Bender F, Ganseman CG, Projogo T. An integrated friction model structure with improved presliding behavior for accurate friction compensation. *IEEE Transact Automat Contr*. 2000;45(4):675-686. https://doi.org/10.1109/9.847103

14. Karnopp D. Computer simulation of stick-slip friction in mechanical dynamic systems. *J DYN Syst, Meas, Control*. 1985;107(1):100-103.

15. Tan X, Rogers R. Dynamic friction modelling in heat exchanger tube simulations. *ASME, Flow-Induced Vibration*. 1996;328.

16. Tariku FA, Rogers RJ. Improved dynamic friction models for simulation of one-dimensional and two-dimensional stick-slip motion. *J Tribol*. 2000;123(4):661-669. https://doi.org/10.1115/1.1331057

17. Antunes J, Axisa F, Beaufils B, Guilbaud D. Coulomb friction modelling in numericalsimulations of vibration and wear work rate of multispan tube bundles. *J Fluid Struct*. 1990;4(3):287-304.

18. Gazetas G, Garini E, Anastasopoulos I, Georgarakos T. Effects of near-fault ground shaking on sliding systems. *J Geotech Geoenviron Eng*. 2009;135(12):1906-1921. https://doi.org/10.1061/(ASCE)GT.1943-5606.0000174

19. Gazetas G, Garini E, Berrill JB, Apostolou M. Sliding and overturning potential of Christchurch 2011 earthquake records. *Earthq Eng Struct D*. 2012;41(February):1921-1944. https://doi.org/10.1002/eqe

20. Westermo B, Udwadia F. Periodic response of a sliding oscillator system to harmonic excitation. *Earthq Eng Struct D*. 1983;11(1):135-146. https://doi.org/10.1002/eqe.4290110111

21. Sorine M. Applications of hysteresis models: Contact friction in tires, muscle contraction. IEEE CDC 98 Workshop, 1998.

22. Velenis E, Tsiotras P, Canudas De Wit C. Extension of the lugre dynamic tire friction model to 2D motion. In: *Proceedings of the 10th IEEE Mediterranean Conference on Control and Automation-MED2002*; 2002.

23. Federal Emergency Management Agency (FEMA). *Quantification of building seismic performance factors*. FEMA P-695. Washington, D.C; 2009.

24. ASCE. *Minimum Design Loads for Buildings and Other Structures, ASCE Standard ASCE/SEI 7–05, including Supplement No. 1*, American Society of Civil Engineers, Reston, Virginia. 2002. https://doi.org/10.1061/9780784412916.

25. Sarma SK, Scorer M. The effect of vertical accelerations on seismic slope stability. Proceedings of the International Conference on Performance Based Design in Earthquake Geotechnical Engineering IS-Tokyo, 1990. https://doi.org/10.13140/2.1.2814.3045.

26. Wu T-Y, El-Tawil S, McCormick J. Highly Ductile Limits for Deep Steel Columns. *Journal of Structural Engineering 144.4*. 2018:04018016.

27. Federal Emergency Management Agency (FEMA). *Seismic Performance Assessment of Buildings. vol. 1*. FEMA P-58. Washington, D.C; 2012.

How to cite this article: Na Y, El-Tawil S, Ibrahim A, Eltawil A. Dynamic behavior of a smart device on a surface subjected to earthquake motion. *Earthquake Engng Struct Dyn*. 2018;47:1905–1920. https://doi.org/10.1002/eqe.3048